Discrimination of β-1,4 and β-1,3 linkages in native oligosaccharides via charge transfer dissociation mass spectrometry.

Hagen Buck-Wiese[1,2,3]; Mathieu Fanuel[4,5]; Manuel Liebeke[2]; Kim Le Mai Hoang[6]; Alonso Pardo-Vagas[6]; Peter H. Seeberger[6,7]; Jan-Hendrik Hehemann[1,3]; Hélène Rogniaux[4,5]; Glen P. Jackson[8,9]*; David Ropartz[4,5]*

[1]MARUM MPG Bridge Group Marine Glycobiology, Max-Planck-Institute for Marine Microbiology, Celsiusstrasse 1, 28359 Bremen, Germany

[2]Research Group Metabolic Interactions, Department of Symbiosis, Max-Planck-Institute for Marine Microbiology, Celsiusstrasse 1, 28359 Bremen, Germany

[3]Marine Glycobiology, Marum Center for Marine Environmental Sciences, Leobener Strasse 8, 28359 Bremen, Germany

[4]INRAE, UR BIA, F-44316 Nantes, France

[5]INRAE, BIBS facility, F-44316 Nantes, France

[6]Max-Planck-Institute of Colloids and Interfaces, Department of Biomolecular Systems, Am Mühlenberg 1, 14476 Potsdam, Germany.

[7]Institute for Chemistry and Biochemistry, Free University Berlin, Arnimallee 22, 14195 Berlin, Germany

[8]Department of Forensic and Investigative Science, West Virginia University, Morgantown, WV 26506, USA

[9]C. Eugene Bennett Department of Chemistry, West Virginia University, Morgantown, WV 26506, USA

Address reprint requests to Dr. Glen P. Jackson, PhD, Dept. of Forensic and Investigative Science, West Virginia University, Morgantown, WV 26506-6121, USA, Email: glen.jackson@mail.wvu.edu, Tel: +01 304-293-9236

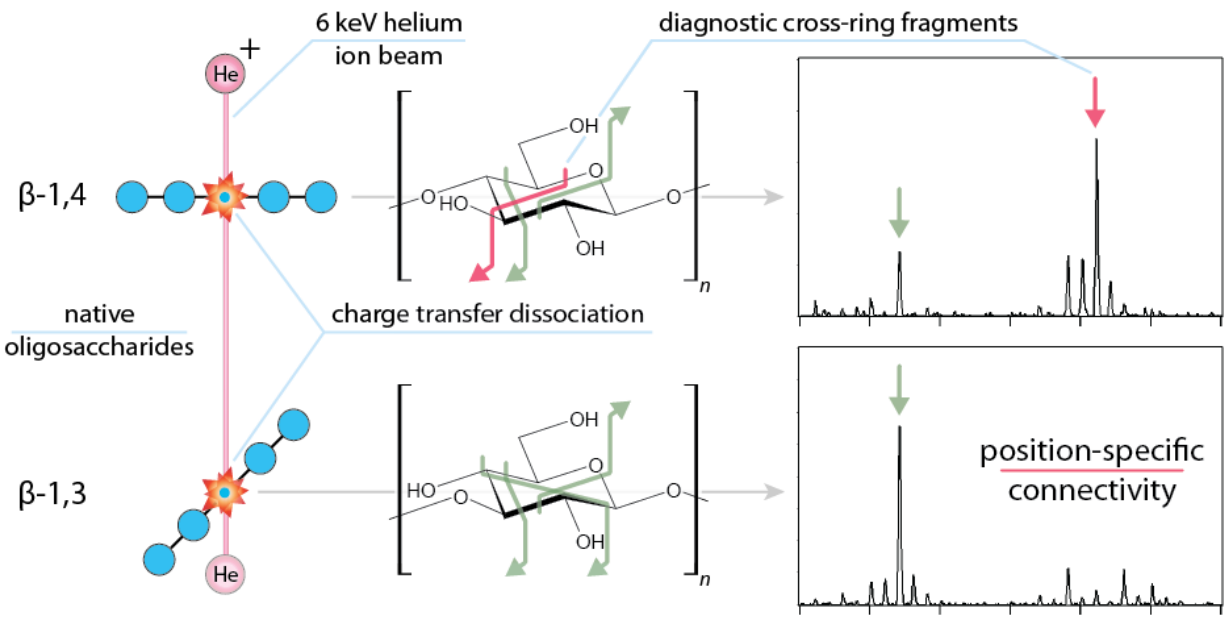

Abstract. The connection between monosaccharides influences the structure, solubility and biological function of carbohydrates. Although tandem mass spectrometry (MS/MS) often enables the compositional identification of carbohydrates, traditional MS/MS fragmentation methods fail to generate abundant cross-ring fragments of intra-chain monosaccharides that could reveal carbohydrate connectivity. We examined the potential of helium-charge transfer dissociation (He-CTD) as a method of MS/MS to decipher the connectivity of β-1,4 and β-1,3 linked oligosaccharides. In contrast to collision-induced dissociation (CID), He-CTD of isolated oligosaccharide precursors produced both glycosidic and cross-ring cleavages of each monosaccharide. The radical-driven dissociation in He-CTD induced single cleavage events, without consecutive fragmentations, which facilitated structural interpretation. He-CTD of various standards up to a degree of polymerization of 7 showed that β-1,4- and β-1,3-linked carbohydrates can be distinguished based on diagnostic ^{3,5}A fragment ions that are characteristic for β-1,4 linkages. Overall, fragment ion spectra from He-CTD contained sufficient information to infer the connectivity specifically for each glycosidic bond. When testing He-CTD to resolve the order of β-1,4- and β-1,3-linkages in mixed-linked oligosaccharide standards, He-CTD spectra sometimes provided less confident assignment of connectivity. Ion mobility spectrometry-mass spectrometry (IMS-MS) of the standards indicated that ambiguity in the He-CTD spectra was caused by isobaric impurities in the mixed-linked oligosaccharides. Radical-driven dissociation induced by He-CTD can thus expand MS/MS to carbohydrate linkage analysis, as demonstrated by the comprehensive fragment ion spectra on native oligosaccharides. The determination of connectivity in true unknowns would benefit from the separation of isobaric precursors, through UPLC or IMS, before linkage determination via He-CTD.

Introduction

Branching, modifications and stereochemistry of carbohydrate structures contribute to their versatile roles in biology.[1] A mere shift in the connectivity of glycosidic bonds can result in substantial differences in structure, solubility and biological function between two oligomers. For example, laminarin and cellulose are both β-linked linear polymers of glucose; however, the β-1,3 linkages in laminarin make it flexible and soluble, which supports its role as energy storage in algae,[2] whereas the β-1,4 linkages in cellulose make it a rigid, insoluble, crystalline fiber supporting its function as a major cell-wall component in plants.[2] Similar stereochemical linkage differences in linkage from β-1,3 to β-1,4 provide the difference between histo-blood types 1 and 2 in human tissues.[3, 4] Despite the importance and apparent simplicity in describing the linkage differences between structures like laminarin and cellulose, it is surprisingly difficult to assess the linkage order of carbohydrates using common analytical approaches for oligomers any longer than two or three sugar units in length.

Whereas bulk glycosyl linkage analysis of permethylated and depolymerized glycans by gas chromatography-mass spectrometry can elucidate the average proportion of different linkages in a carbohydrate polymer, the initial depolymerization step eliminates the ability to elucidate the sequence of the linkages.[5, 6] For example, using bulk glycosyl-linkage analysis methods like GC-MS, a polymer of glucose with the repeated sequence $(\beta\text{-}1,3)_2(\beta\text{-}1,4)_2$ would be indistinguishable from the sequence $(\beta\text{-}1,3, \beta\text{-}1,4)_2$ because both contain an equal proportion of β-1,3 and β-1,4 linkages. This shortcoming of complete depolymerization for GC-MS has led to the development of liquid chromatography-mass spectrometry (LC-MS) techniques that enable the separation of stereoisomers of carbohydrates,[7] and LC-MS requires only partial depolymerization of polymers into oligomers before the analysis. The distinction of linkages using LC-MS necessitates tandem mass spectrometry (MS/MS) strategies because the oligomers typically exhibit similar or identical molecular masses.

To distinguish and identify separated carbohydrate isomers, MS/MS aims to produce informative fragments from the precursor ions. During collisional activation of isolated precursors in MS/MS[8] energy moves freely within the molecule and induces cleavage at the weakest bonds.[7, 9-12] In carbohydrates, the weakest bonds are usually the glycosidic bonds. This bias towards glycosidic bond cleavage is useful for determining the sequence order of mixed sugar sequences but limits the ability to infer connectivity or to distinguish aldohexoses from one another. In contrast to the lower energy rearrangements of CID, techniques like electron-induced dissociation (ExD), ultraviolet photodissociation (UVPD) or helium-charge transfer dissociation (He-CTD) tend to produce fragments with higher energy radical-driven cleavages.[11,

[13-18] These radical-driven techniques produce fragments that are more informative than CID about the structure and stereochemistry of the activated molecule.

Cross-ring cleavages by radical-driven dissociation methods permit detailed structural analyses of carbohydrates, but unambiguous linkage determination requires many informative cross-ring fragments, which is not always possible. ExD is typically the most reliable and informative approach to cross-ring cleavages, but ExD is typically restricted to high-end FT-ICR mass spectrometers, and even ExD encounters limitations in the variety of induced cleavages.[14, 15, 18-20] UVPD has been highly informative, but it does not consistently produce sufficient cross-ring fragments for a linkage determination to be routinely achievable.[21, 22] However, experiments on carbohydrates using He-CTD demonstrate effective fragmentation with abundant cross-ring cleavages, the maintenance of labile sulfate modifications [23] and the absence of consecutive fragmentation.[23, 24] The last two studies established the performance of He-CTD for structural determination of carbohydrates, although they did not specifically address the issue of linkage determination.

Here, we work on the hypothesis that radical-driven He-CTD can provide a sufficient array of cross-ring cleavages to resolve the connectivity in carbohydrates. To test this hypothesis, oligomers of laminarin and cellulose with a degree of polymerization of between DP4-DP7 were analyzed in their isolated forms using electrospray ionization. Each oligomer was isolated in the 3D ion trap and fragmented as $[M+Na]^+$ species without permethylation or derivatization. Most of the results describe observations on DP4 and DP5. For comparison purposes, the same oligomers were analyzed on the same instrument in pseudo-real time using either He-CTD or CID. In a typical spectrum of a DP4 oligomer, He-CTD produced more than 80 peaks from the $[M+Na]^+$ precursor compared to less than 20 peaks using CID. Peaks from He-CTD corresponded to B/Y, C/Z, and A/X ions, the latter of which originated from various cross-ring cleavage sites and distinguished β-1,4 linkages in cellulose from β-1,3 linkages in laminarin. He-CTD, but not CID, succeeded in determining the positions of β-1,3 and β-1,4 linkages in three mixed-linked tetrasaccharides. This capability makes He-CTD a unique analytical tool for mass spectrometry-based carbohydrate research.

Experimental

Analytes

Cellulose and laminarin oligosaccharides with degree of polymerization (DP) 3 through 6, and mixed linked tetrasaccharides were obtained from Megazyme (Bray, Ireland). Laminarin DP7 was prepared by automated glycan assembly.[25] For all electrospray (ESI) analyses, solutions of 1 µg mL^{-1} were prepared in 1/1 (v/v) methanol/water and injected at 5 µL min^{-1} flow rate.

Helium-charge transfer dissociation (He-CTD)

He-CTD mass spectra were obtained on a Bruker amaZon 3D ion trap (amaZon SL, Bruker Daltonics, Bremen, Germany) interfaced with a saddle field fast ion source (VSW/Atomtech, Macclesfield, UK) with UHP helium as the CTD reagent gas. The flow of helium from the ion gun to the main vacuum chamber raised the base pressure from ~$8x10^{-6}$ mbar to ~$1.2x10^{-5}$ mbar. The ion beam flux was on the order of 5 µA. Singly charged precursor ions were isolated as sodium adducts in positive mode using a window of 2 Da. Ion accumulation times were typically on the order of 0.5 msec for CID and 5 msec for CTD. Although the 5-msec accumulation time ordinarily causes deleterious space charge conditions, the unreacted precursors were resonantly ejected using a 5 V ejection amplitude after the CTD reaction and before mass acquisition to maximize the signal to noise ratio of the product ion spectra while negating the space charge that the unreacted precursors would cause. The CTD beam was pulsed on for 170 msec using a 6-keV potential to provide a beam of ~5.1 keV helium ions with a low mass cut off of 250 Da. CTD product ion spectra were recorded for 1-2 min over a *m/z* range of 200-1500.

Data treatment

Raw files were converted into mzML format using MSConvert (http://proteowizard.sourceforge.net/tools.shtml) and averaged using mMass version 5.5.0.[26-28] Averaged spectra were normalized to the most intense peak. Peak picking was performed using a threshold signal-to-noise ratio of 5 and a minimum relative intensity of 1%, with inbuilt tools for baseline correction, smoothing and deisotoping active. Peaks were annotated according to the nomenclature of Domon and Costello[29] using a compound library created in R version 3.6.1[30] (Table S1), and the annotation function in mMass with a tolerance of 0.1 Da. For the figures, spectra were exported from mMass as PNG files and processed in Adobe Illustrator CS5.

Ion mobility

For the cellulose DP4 and the three mixed linked tetrasaccharides, arrival time distributions were measured using a Synapt G2Si HDMS (Waters, Manchester, UK) in positive ionization mode over the mass

range of *m/z* 300-1200. The four tetrasaccharides were isolated using the quadrupole at *m/z* 689.2 as $[M-Na]^+$ and were separated in the TWIM cell using nitrogen (99.9999%, 90 ml min^{-1}) as the drift IMS gas after cooling in the helium cell (99.9999%, 180 mL min^{-1}). The signal was recorded for 0.5 min at a constant wave velocity of 550 m sec^{-1}. Data acquisition and analysis were performed using MassLynx 4.1 (Waters, Manchester, UK).

Results and discussion

Linkage determination in oligomers with homogeneous linkages

Almost all of the hypothetical glycosidic and cross-ring cleavages of cellulose share an isobaric analog ion with laminarin. The only exceptions are the $^{3,5}A_n$ ion of cellulose and the isobaric $^{0,3}X_n$ and $^{3,5}X_n$ ions for cellulose, which share no theoretical isobars with laminarin. We tested the ability of He-CTD and CID to form the hypothetically unique fragments for cellulose relative to laminarin. First, we fragmented cellulose DP4, which has four β-1,4-linked glucose units using either He-CTD or CID. He-CTD produced 88 peaks from the cellulose DP4 precursor ($[M+Na]^+$, $C_{24}H_{42}O_{21}Na$, *m/z* 689.21), whereas CID only produced 16 peaks. The peak assignments for He-CTD and CID are summarized in Table 1.

Table 1: Fragment ions from He-CTD and CID on cellulose DP4. The added symbol '' to a fragment ion indicates an extra H_2 loss. Nomenclature following Domon and Costello.[29]

	Annotation	Relative intensity (%)			Annotation	Relative intensity (%)	
m/z	**(0.1 Da tolerance)**	**CTD**	**CID**	***m/z***	**(0.1 Da tolerance)**	**CTD**	**CID**
228.99	$^{1,5}X_1$''	2.40		405.04	$^{0,2}X_2$''/$^{2,4}A_3$''	1.40	
230.99	$^{1,5}X_1$	39.19		407.07	$^{0,2}X_2$/$^{2,4}A_3$	8.72	2.67
243.00	$^{0,2}X_1$''/$^{2,4}A_2$''	2.05		419.07	$^{3,5}A_3$''	7.67	
245.00	$^{0,2}X_1$/$^{2,4}A_2$	9.75		421.09	$^{2,5}X_2$''/$^{3,5}A_3$	11.57	
257.01	$^{3,5}A_2$''	4.57		435.06	$^{1,4}X_2$''/$^{1,4}A_3$''/$^{0,3}A_3$''	4.03	
259.02	$^{2,5}X_1$''/$^{3,5}A_2$	15.68		437.07	$^{1,4}X_2$/$^{1,4}A_3$/$^{0,3}A_3$	3.47	
261.00	$^{2,5}X_1$	1.62		449.07	2,5A''	6.00	1.83
273.00	$^{1,4}X_1$''/$^{1,4}A_2$''/$^{0,3}A_2$''	5.66		465.07	$^{2,4}X_2$''/$^{0,2}A_3$''	2.51	
275.03	$^{1,4}X_1$/$^{1,4}A_2$/$^{0,3}A_2$	1.97		467.09	$^{2,4}X_2$/$^{0,2}A_3$	4.20	6.52
287.03	$^{2,5}A_2$''	13.26		479.08	$^{1,5}A_3$''	4.07	
289.02	$^{2,5}A_2$	1.52		481.11	$^{1,5}A_3$	1.43	
303.03	$^{2,4}X_1$''/$^{0,2}A_2$''	2.73		507.05	B_3''	3.81	
305.05	$^{2,4}X_1$/$^{0,2}A_2$	6.70	3.48	509.08	B_3/Z_3	22.42	100.00
317.05	$^{1,5}A_2$''	7.94		525.08	C_3''/Y_3''	19.67	
319.04	$^{1,5}A_2$	2.06		527.09	C_3/Y_3	28.31	29.11
345.04	B_2''	4.41		553.09	$^{1,5}X_3$''	1.49	
347.06	B_2/Z_2	51.55	39.32	555.07	$^{1,5}X_3$	57.62	
349.07	Z_2''	2.29		569.10	$^{0,2}X_3$/$^{2,4}A_4$	3.27	33.24
363.05	C_2''/Y_2''	35.60		583.09	$^{2,5}X_3$''/$^{3,5}A_4$	3.29	
365.07	C_2/Y_2	49.25	21.72	611.11	$^{2,5}A_4$''		1.14
391.03	$^{1,5}X_2$''	7.85		629.09	$^{2,4}X_3$/$^{0,2}A_4$	1.53	61.35
393.05	$^{1,5}X_2$	100.00		671.12	B_4/Z_4		41.99

In the He-CTD spectrum of cellulose DP4 (Figure 1a), major peaks corresponded to cross-ring cleavages, which tended to be of the type $^{1,5}X_n$ and $^{3,5}A_n$, as well as glycosidic bond cleavages. Less abundant ions in the He-CTD spectra included cross-ring cleavages of the types $^{2,4}A_n/^{0,2}X_{n-1}$, $^{2,5}X_n$, $^{2,5}A_n$, $^{1,5}A_n$, and $^{0,3}A_n/^{1,4}A_n/^{1,4}X_{n-1}$. Ions separated by a forward slash, e.g. $^{2,4}A_n/^{0,2}X_{n-1}$, are isobars that cannot be unambiguously identified unless one of the termini is altered in such a way as to break the mass symmetry. Fragment ions in the He-CTD spectrum were often accompanied by peaks at -1 and -2 Da, which very likely are the result of extra $H^{\bullet}$ or H_2 losses, respectively.[14, 15, 23, 24] In the CID spectrum of cellulose DP4 (Figure 1b), B and Y fragment ions from glycosidic bond-cleavages dominate, and ions from cross-ring cleavage are restricted to the types $^{2,4}A_n/^{0,2}X_{n-1}$ and $^{0,2}A_n/^{2,4}X_{n-1}$ (Table 1). Cross-ring cleavages of the type $^{0,2}X_{n-1}$ and $^{0,2}A_n$ are essentially uninformative. In contrast to CID, He-CTD yielded cross-ring fragment ions of a variety of positions of all glucose units, which provided information on the connectivity of the glycosidic bonds along the complete backbone.

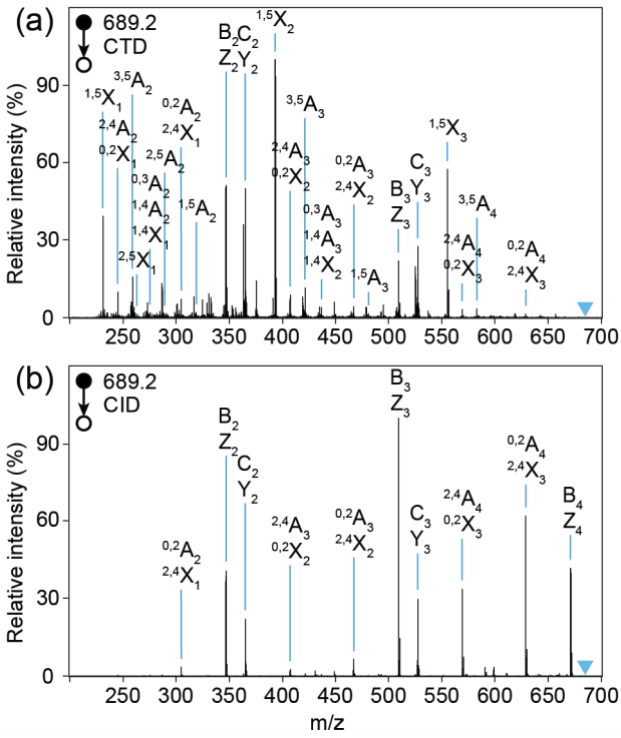

Figure 1: Fragment ion spectra of cellulose DP4 ($[M+Na]^+$, $C_{24}H_{42}O_{21}Na$, *m/z* 689.21)**.** a) He-CTD, b) CID. Annotations following the nomenclature of Domon and Costello.[29] Blue triangles indicate the *m/z* of the resonantly ejected precursor.

Fragmentation spectra of He-CTD on cellulose DP5 and laminarin DP5 (both $[M+Na]^+$, $C_{30}H_{52}O_{26}Na$, *m/z* 851.26) are displayed in Figures 2 and 3, respectively. Note that, as described above, unreacted precursor ions are not visible at *m/z* 851.26, because they have been resonantly ejected before mass acquisition. As observed before for cellulose DP4, the He-CTD spectra for cellulose DP5 and laminarin DP5 are rich in cross-ring cleavages. We explored those spectra to find a signature of the different connectivity of the two structures. In theory, a $^{3,5}A$ fragment cannot be formed by 1,3-linked carbohydrates (see Table S1 in the Supplementary Information SI). Thus, $^{3,5}A_n$ fragments should be produced only in the case of the cellulose (all β-1,4) DP5 product and not for laminarin (all β-1,3) DP5. Indeed, He-CTD fragmentation of cellulose DP5 yielded a consistent series of $^{3,5}A_n$ fragments (Figure 2c-f). In contrast, very minor peaks were present at same *m/z* values of $^{3,5}A_n$ peaks in He-CTD fragment spectra of laminarin DP5 (Figure 3c-f). To determine whether these peaks stemmed from isobaric fragments such as $^{2,5}X_{n-1}$'', or from contamination,

we compared the commercially available laminarin DP5 to a synthesized laminarin DP7 of high purity. He-CTD on the synthesized laminarin DP7 ($[M+Na]^+$, $C_{42}H_{72}O_{36}Na$, *m/z* 1175.37) yielded very similar fragment ion spectra compared to the laminarin DP5 (Figure 4), including the minor peaks at the *m/z* of $^{3,5}A_n$. Notably, the ratio of the intensity of $^{3,5}A_n$ over the sum of isobaric $^{1,3}A_n/^{2,4}A_n/^{0,2}X_{n-1}$ ions ranged between 1.6 and 2.7 for β-1,4 bonds, but remained consistently below 0.2 for β-1,3 bonds (Figures 2c-f, 3c-f and 4b-e).

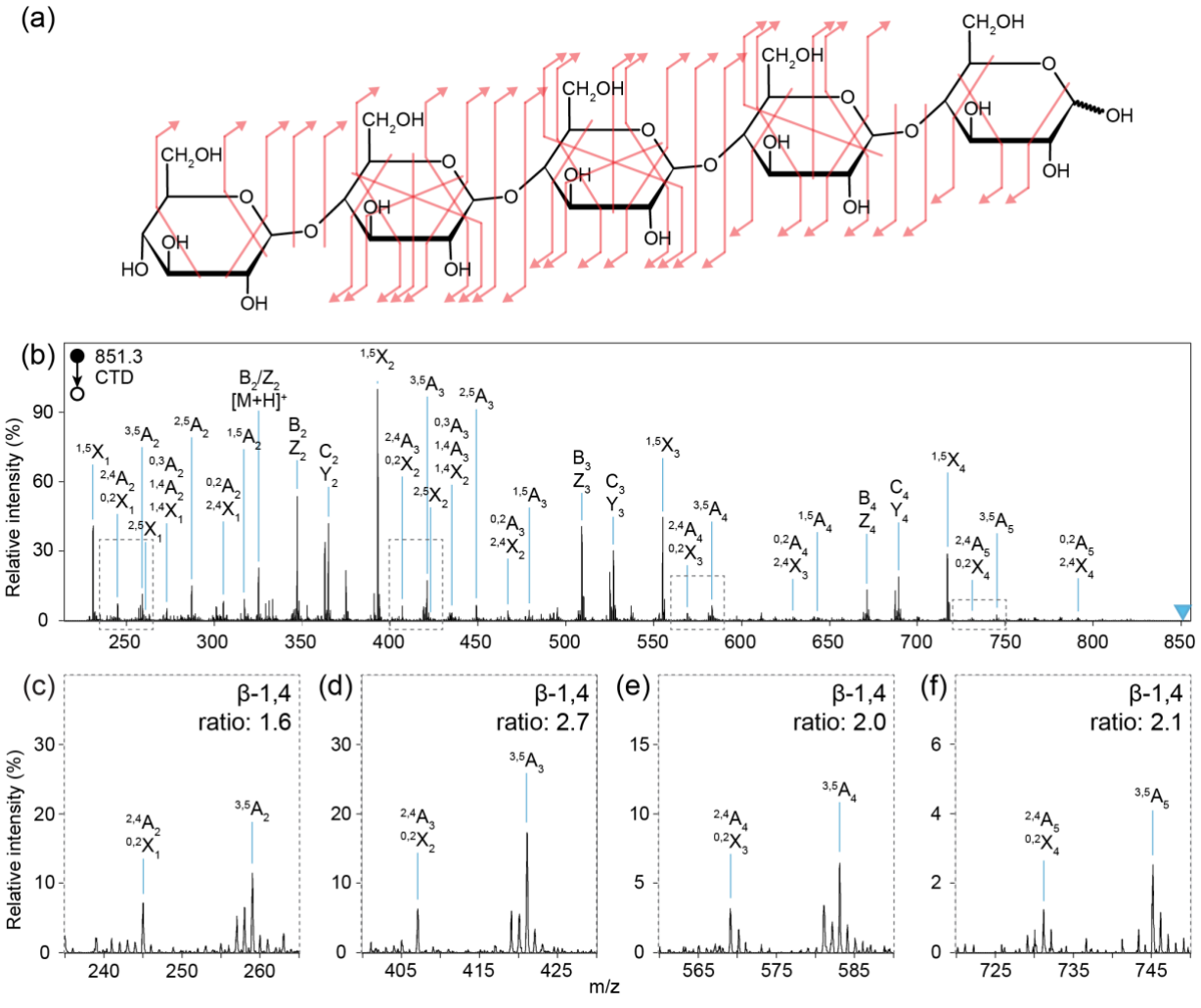

Figure 2: Fragmentation pattern indicative of a 1,4 glycosidic linkage from He-CTD on cellulose DP5. a) Structure of cellulose DP5 with observed cleavages in red. b) Fragment ions generated from cellulose DP5 ($[M+Na]^+$, $C_{30}H_{52}O_{26}Na$, 851.26). c-f) Magnified regions show $^{3,5}A_n$ fragment ions and ratio of $^{3,5}A_n$ over $^{2,4}A_n/^{0,2}X_{n-1}$ fragment ions characteristic of 1,4 linkages. Annotations following the nomenclature of Domon and Costello.[29] The blue triangle indicates the *m/z* of the resonantly ejected precursor.

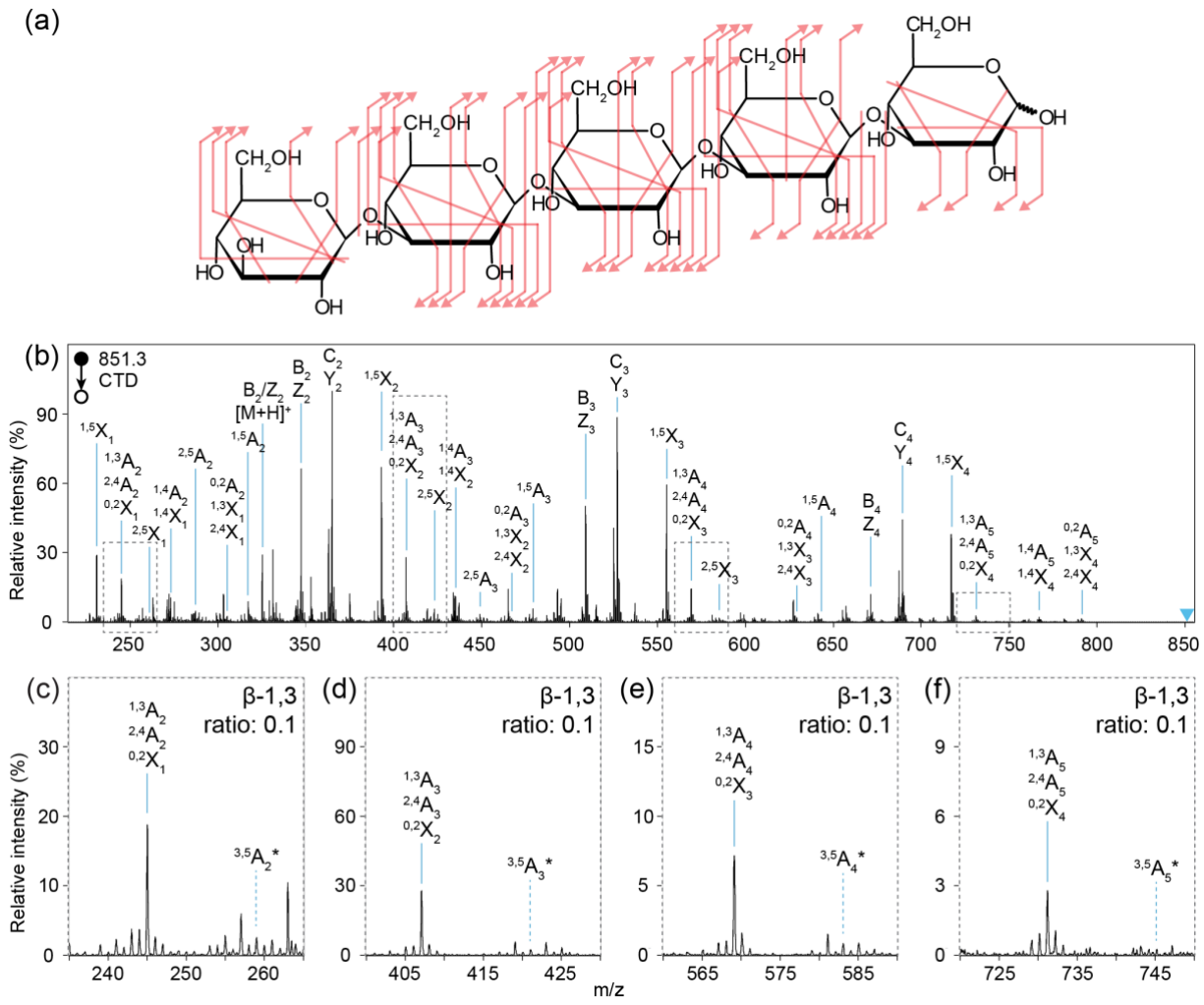

Figure 3: Fragmentation pattern indicative of a 1,3 glycosidic linkage from He-CTD on laminarin DP5. a) Structure of laminarin DP5 with observed cleavages in red. b) Fragment ions generated from laminarin DP5 ($[M+Na]^+$, $C_{30}H_{52}O_{26}Na$, *m/z* 851.26). c-f) Magnified regions show ratio of peak at m/z of $^{3,5}A_n$ over $^{1,3}A_n/^{2,4}A_n/^{0,2}X_{n-1}$ fragments characteristic of 1,3 linkages. Annotations following nomenclature of Domon and Costello.[29] The blue triangle indicates the *m/z* of the resonantly ejected precursor. The $^{3,5}A_n^*$ labels with an asterisk indicate that these fragments are only possible for a β-1,4 linkage at these positions.

A 1,4-linked carbohydrate could hypothetically produce $^{0,3}X_n$ and $^{3,5}X_n$ fragments, whereas a 1,3-linked carbohydrate cannot. However, neither the He-CTD product ion spectra of cellulose nor laminarin provided any notable $^{0,3}X_n/^{3,5}X_n$ fragment ions. The absence of $^{0,3}X_n/^{3,5}X_n$ fragments in He-CTD spectra is consistent with observations from electron-induced dissociation [14] of similar substrates. In radical-driven fragmentation techniques, $^{0,3}X$ and $^{3,5}X$ cleavages are believed to form via a diradical, which then undergoes β-elimination to form a $^{1,5}X$ fragment.[14] The higher intensity of $^{1,5}X_n$ fragments for cellulose (Figures 1a and 2b) compared to laminarin (Figures 3b and 4) supports this theory of β-elimination. In

contrast to laminarin, He-CTD of cellulose likely does form $^{0,3}X_n$ and $^{3,5}X_n$ fragments, which probably rapidly undergo β-elimination to form $^{1,5}X_n$ fragments. Resonance ejection experiments (described later) confirm that any consecutive fragmentations during He-CTD occur on the timescale that is faster than the time required for a primary product ion to obtain an unstable trajectory in the trap, which is on the order of a few rf oscillations at ~1 MHz, or ~50 μs.[31]

In contrast to the unique $^{3,5}A_n$ ions for cellulose, laminarin can theoretically form $^{1,3}A_n$ fragments, whereas cellulose cannot. However, the $^{1,3}A_n$ fragments of laminarin are isobaric with the $^{2,4}A_n$ and $^{0,2}X_{n-1}$ fragments of cellulose, so there are no unique mass fragments indicative of 1,3 linkages. Note, however, that when the $^{1,3}A_n$ fragment of laminarin coincides with the isobaric $^{2,4}A_n$ and $^{0,2}X_{n-1}$ fragments, laminarin provides peaks with a higher intensity for the combined $^{1,3}A_n/^{2,4}A_n/^{0,2}X_{n-1}$ peak than does cellulose for $^{2,4}A_n/^{0,2}X_{n-1}$ (Figures 2 and 3). The theoretical differences between cross-ring cleavages of cellulose and laminarin predict that the ratio of the abundance at $^{1,3}A_n/^{2,4}A_n/^{0,2}X_{n-1}$ to $^{3,5}A_n$ should be greatest for laminarin and the smallest for cellulose. Finally, $^{1,4}A_n/^{1,4}X_{n-1}$ fragment ions were less abundant in the He-CTD spectrum of cellulose when compared to laminarin, despite isobaric $^{0,3}A_n$ fragments that could theoretically be formed by cellulose, but not by laminarin. To our surprise, the intensity of the $^{1,4}A_n/^{1,4}X_{n-1}$ fragments from laminarin were consistently >2x the intensity of $^{0,3}A_n/^{1,4}A_n/^{1,4}X_{n-1}$ fragments from cellulose (Figures 2b and 3b). Relative to β-1,4-glycosidic linkages, the β-1,3-glycosidic linkage must favor 1,4 cross-ring cleavages. The consistent differences in fragment ion intensities from He-CTD spectra of cellulose and laminarin of different DPs demonstrate the dependency of cross-ring fragments on linkage position and may enable computational methods for carbohydrate identification.

In CID, the elevated internal energy of a precursor ion is randomized throughout the ion and consecutive fragmentation reactions are quite common because the primary product ions can be created with an excess of internal energy.[31] Consecutive fragmentations are an expected part of the quazi-equilibrium theory of unimolecular fragmentation.[11, 32-34] Such consecutive reactions are obviated, or at least less common, in non-ergodic fragmentations induced by electron activation.[35] In the present study, our conclusion about connectivity relies on signature fragments such as $^{3,5}A_n$ ions, and any consecutive fragmentation during He-CTD could jeopardize our approach to infer connectivity from fragment ions by creating uncertainty on the origin of these fragments.

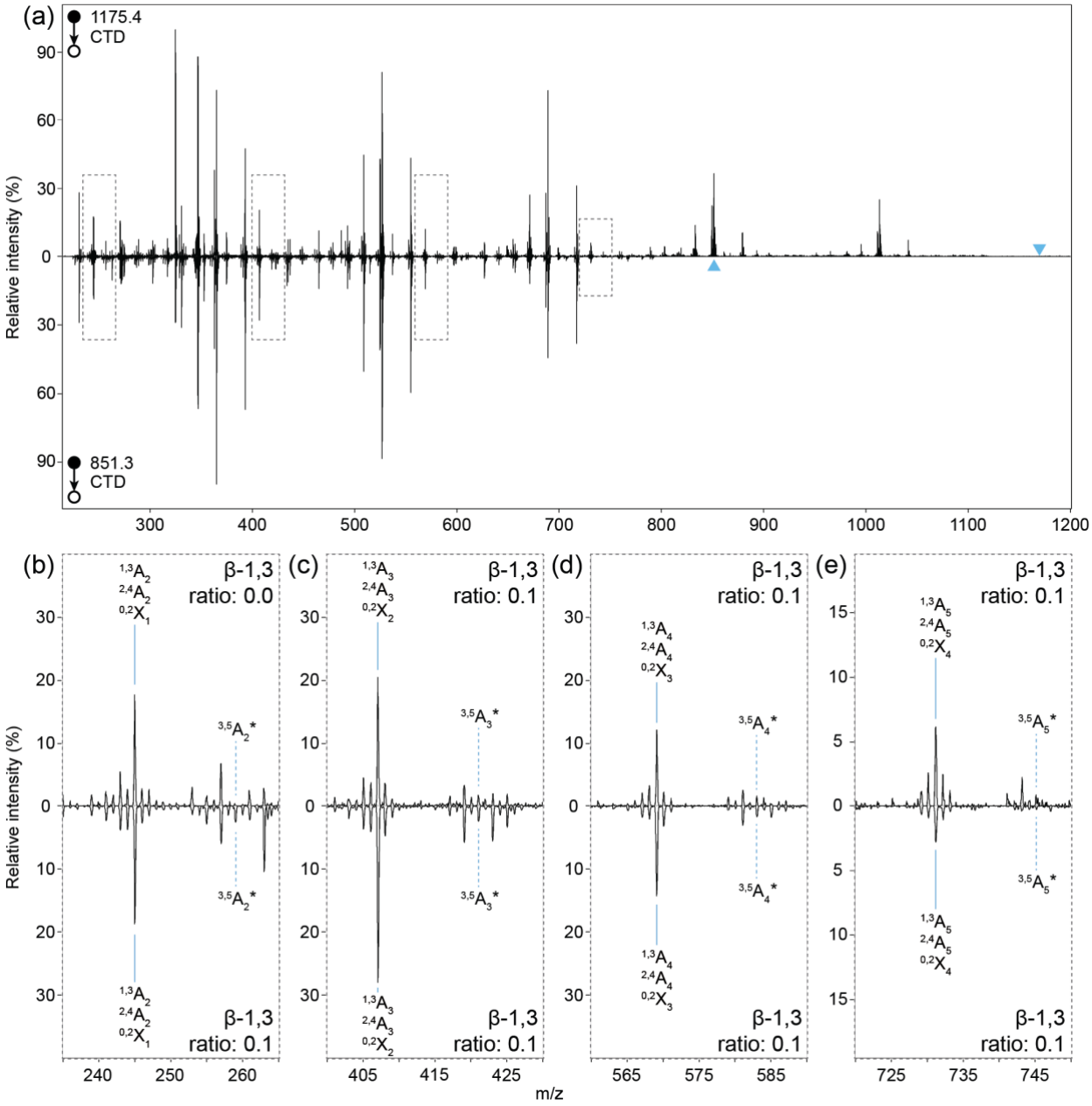

Figure 4: He-CTD on solid-phase-synthesized laminarin DP7 of high purity and commercially available laminarin DP5. a) Fragment ion spectrum of laminarin DP7 ($[M+Na]^+$, $C_{42}H_{72}O_{36}Na$, 851.26) on top and fragment ion spectrum of fragment ion spectrum of laminarin DP5 ($[M+Na]^+$, $C_{30}H_{52}O_{26}Na$, 851.26) below. b-e) Magnified regions show ratio of peak at m/z of $^{3,5}A_n$ over $^{1,3}A_n/^{2,4}A_n/^{0,2}X_{n-1}$ fragments characteristic of 1,3 linkages for laminarin DP7 on top and laminarin DP5 below. Annotations following the nomenclature of Domon and Costello.[29] Blue triangles indicate the *m/z* of the resonantly ejected precursor. The $^{3,5}A_n^*$ labels with an asterisk indicate that these fragments are only possible for a β-1,4 linkage at these positions.

To demonstrate the absence of consecutive fragmentation in He-CTD, we performed resonance ejection experiments of a variety of different primary products during He-CTD (Figure 5). For example, He-CTD of cellulose DP5 ($[M+Na]^+$, *m/z* 851.26) produces an abundant fragment at *m/z* 555 as well as a less

abundant fragment at *m/z* 495 (Figure 5b). Isolation of the He-CTD-product at *m/z* 555 followed by collisional activation at the MS^3 level results in a base peak at *m/z* 495 in the MS^3 spectrum (Figure 5b), which is easily rationalized by the loss of 60 Da ($C_2O_2H_4$). The fact that the fragment at *m/z* 555 *can* undergo consecutive fragmentation to *m/z* 495 provides uncertainty in the relative proportion of *m/z* 495 that is formed directly or via an intermediate fragment such as the one at *m/z* 555. However, resonant ejection of *m/z* 555 during He-CTD did not cause any significant decrease in the abundance of the *m/z* 495, nor of any other known CID products of *m/z* 555 (Figure 5b). Therefore, the fragment ions observed in the He-CTD spectrum must result from direct cleavages, or consecutive fragmentations that are faster than a few rf cycles at ~1 MHz. Similar observations were made on more than six different fragments for laminarin and cellulose.

The lack of consecutive fragmentations in He-CTD, which is experimentally demonstrated here for the first time, permits the exclusion of internal fragments or consecutive fragments when annotating He-CTD product ion spectra. The fragment ions from a single cleavage event in He-CTD facilitate the *in-silico* reconstruction of molecules and to decipher the linkage configuration of each glycosidic bond within a carbohydrate.

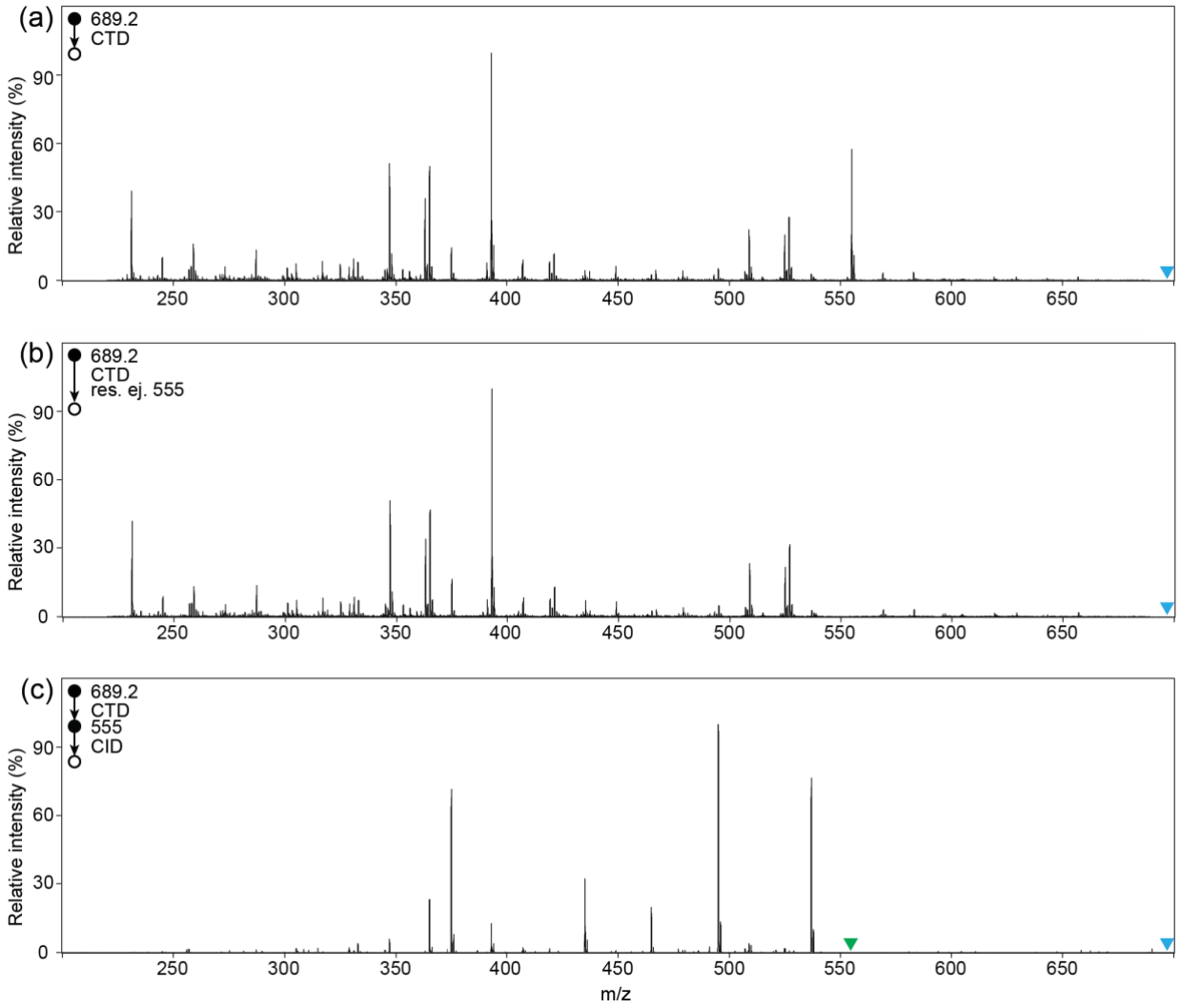

Figure 5: He-CTD spectra of cellulose DP4 to demonstrate the absence of consecutive fragmentation during He-CTD. a) He-CTD of cellulose DP4 ($[M+Na]^+$, $C_{24}H_{42}O_{21}Na$, *m/z* 689.21). b) He-CTD of cellulose DP4 with simultaneous resonance ejection at *m/z* 555. c) He-CTD of cellulose DP4 followed by isolation and resonance excitation (CID) at *m/z* 555±1. Blue triangles indicate the m/z of the resonantly ejected precursor. The green triangle in c) indicates the *m/z* of the isolated and fragmented *m/z* 555 fragment ion.

Linkage determination in structures with mixed linkages

To validate our observations and verify that He-CTD can decipher the connectivity of mixed-linked carbohydrates, we analyzed three commercial mixed-linked tetrasaccharide standards (Figure 6). These isomers each contain two β-1,4 glycosidic bonds and one β-1,3 glycosidic bond, with the β-1,3 glycosidic

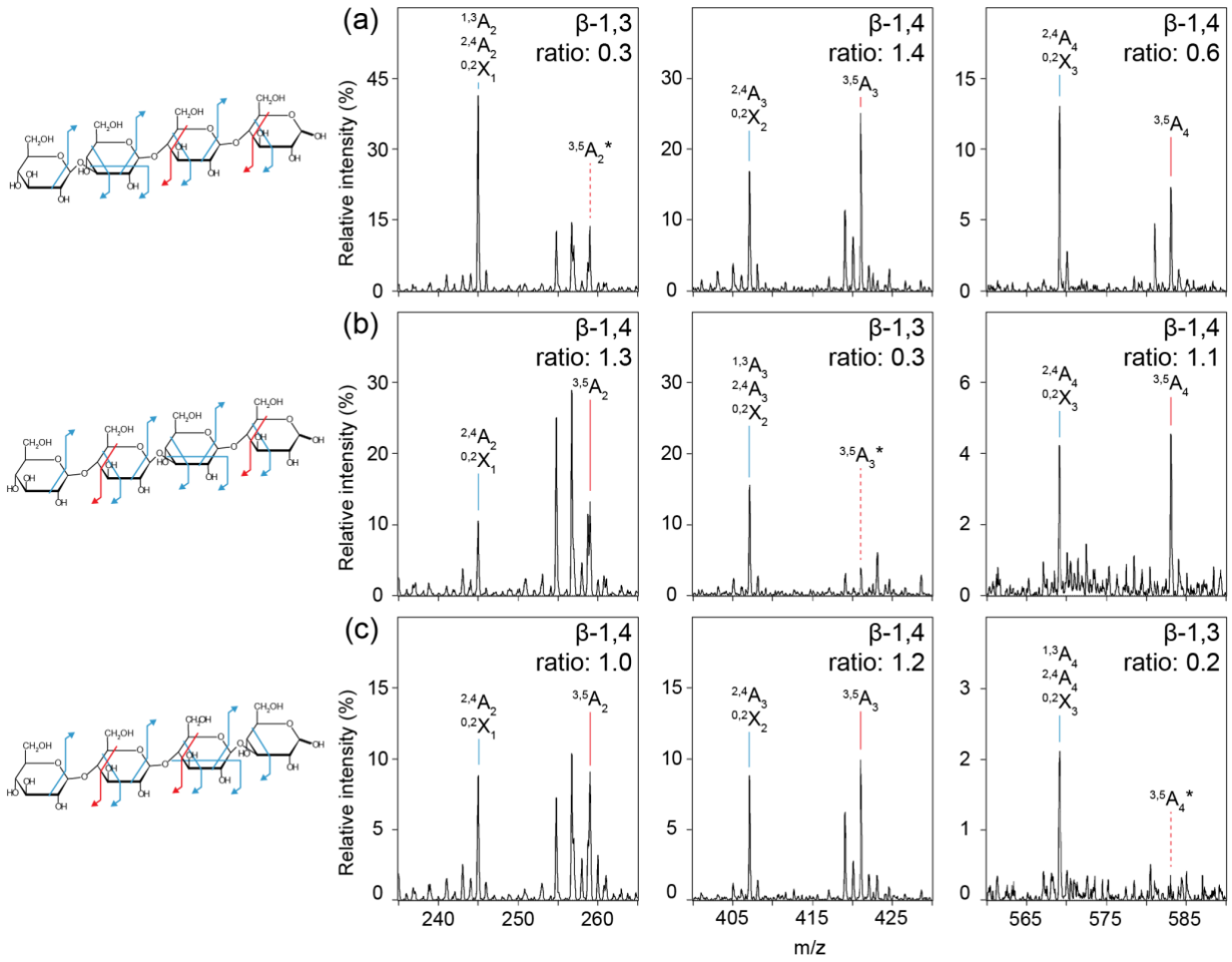

Figure 6: Linkage identification in three stereoisomers of mixed linked glucans via He-CTD. Left: Structures of mixed-linked tetrasaccharides differing in the position of the β-1,3 linkage. a–c) Regions of He-CTD spectra with ratio indicating the $^{3,5}A_n$ over $^{1,3}A_n/^{2,4}A_n/^{0,2}X_n$. $^{1,3}A_n$, $^{2,4}A_n$ and $^{0,2}X_n$ cleavages and fragment ions indicated in blue and $^{3,5}A_n$ cleavages and fragment ions in red. The $^{3,5}A_n{}^*$ labels with an asterisk indicate that these fragments are only possible for a β-1,4 linkage at these positions.

bond in position 1, 2 or 3. Position 1 refers to the glycosidic bond closest to the non-reducing end, position 2 refers to the central glycosidic bond, and position 3 refers to the glycosidic bond furthest away from the non-reducing end and closest to the reducing end. Based on the experiments on cellulose and laminarin, one would expect that a β-1,3 linkage in a certain position would not produce a $^{3,5}A$ fragment ion at that position. Instead, one would expect the β-1,3 link to produce a $^{1,3}A$ fragment ion that enhances the abundance of the isobaric peaks with the identities $^{2,4}A$ and $^{0,2}X$. Moreover, fragments ions can be assigned to originate from a specific cleavage due to the absence of consecutive fragmentation.

For He-CTD of the mixed-linked tetrasaccharides ($[M+Na]^+$, $C_{24}H_{42}O_{21}Na$, *m/z* 689.21), the abundances of the $^{3,5}A_n$ fragment ions are markedly reduced in positions that contain the β-1,3 linkages,

whereas the $^{3,5}A_n$ fragments are similar or greater in abundance than the corresponding $^{1,3}A_n/^{2,4}A_n/^{0,2}X_{n-1}$ ions in positions that contain the β-1,4 linkages (Figure 6). For example, the first panel in Figure 6a is of He-CTD of the tetrasaccharide with the linkages in the order β-1,3/ β-1,4/ β-1,4. At the β-1,3 linkage, the abundance of the $^{3,5}A_2$ peak at *m/z* 259 is 0.3x the abundance of the $^{1,3}A_2/^{2,4}A_2/^{0,2}X_1$ peak at *m/z* 245. In contrast, the second panel of Figure 6a shows that, in the first β-1,4 position, the abundance of the $^{3,5}A_3$ peak at *m/z* 421 is 1.4x the abundance of the $^{2,4}A_3/^{0,2}X_2$ peak at *m/z* 417. In all but one case, the abundances of the $^{3,5}A_n$ ions at the β-1,4 positions exceed the abundances of the corresponding $^{2,4}A_n/^{0,2}X_{n-1}$ ions.

In contrast to He-CTD, CID on the mixed-linked tetrasaccharides did not yield fragment ions that could reveal the connectivity of the three tetrasaccharides (see Fig. S1 in the Supporting Information SI). For example, the abundance of the $^{2,4}A_2/^{0,2}X_1$ reference peak at *m/z* 245 is very weak; the abundance is consistently less than 1%. In contrast, the He-CTD results in Figure 6 show that the abundance of the same fragments is consistently greater than 7%. Whereas the absence of the corresponding $^{3,5}A_2$ peak at *m/z* 259 in Fig. S1a is correctly indicative of the β-1,3 linkage in this isomer, this indicator of β-1,4 linkages is also unreliably weak in Fig. S1b and c. Another example of the ambiguity of the CID spectra is that the $^{3,5}A_4$ fragments at *m/z* 583 were not observed at all in the two isomers that theoretically can provide this fragment. The absence of any signal for the $^{3,5}A_4$ peak might erroneously lead one to conclude that there might be a β-1,3 linkage at this position. In short, the abundances of the $^{3,5}A_n$ and $^{2,4}A_n/^{0,2}X_{n-1}$ fragments ions in CID were not helpful in differentiating β-1,3 from β-1,4 linkages.

Returning to the He-CTD spectra on the three isomeric tetrasaccharides, we were initially disappointed that the ratios of the $^{3,5}A_n$ to $^{2,4}A_n/^{0,2}X_{n-1}$ products ions were not as unambiguous as the iso-linked cellulose and laminarin standards. For example, the ratio of $^{3,5}A_n$ to $^{2,4}A_n/^{0,2}X_{n-1}$ always exceeded 1.5 in cellulose (Figure 2c-f), but the same β-1,4 linkage in one of the mixed-link tetrasaccharides only provided a ratio of 0.6 (Figure 6a). A hypothetical possibility to explain the abundance at the $^{3,5}A_2$ and $^{3,5}A_3$ ions seen for cellulose in Figure 6a and 6b is through internal fragments such as $Y_2/^{3,5}A_4$ (or $Y_3/^{3,5}A_3$) and $Y^3/^{3,5}A_4$, respectively. If such internal fragments were also possible in the mixed-linkage tetrasaccharides, then CTD of the tetrasaccharide with the β-1,3 in position 3 (Figure 6c) could not generate an internal fragment that is isobaric to $^{3,5}A_4^*$, and thus has the lowest ratio of contaminant cross-ring fragments. However, for such internal fragments to be observed in the resonance ejection experiments described above, the cleavage sites on either end of the internal fragment must occur pseudo-simultaneously. Given that there is no adequate mechanism to explain such simultaneous activation at disparate sites of the precursor in a single collision event, the occurrence of internal fragments in CTD seems less likely than the presence of

288 impurities. Also, previous work with heavy ^{18}O labeling on the reducing terminus of Iota- and Kappa-
289 carrageenans showed that CTD spectra were devoid of internal fragments.[23]

290

291 We, therefore, investigated alternative reasons for the slight ambiguity in the He-CTD spectra of the mixed
292 linked tetrasaccharides compared to our cellulose and laminarin standards. One obvious explanation are
293 isomeric (or isobaric) impurities in the mixed-linked tetrasaccharides. To confirm this hypothesis, ion
294 mobility-mass spectrometry (IM-MS) was performed on the three tetrasaccharides and cellulose DP4

295 (Figure 7).

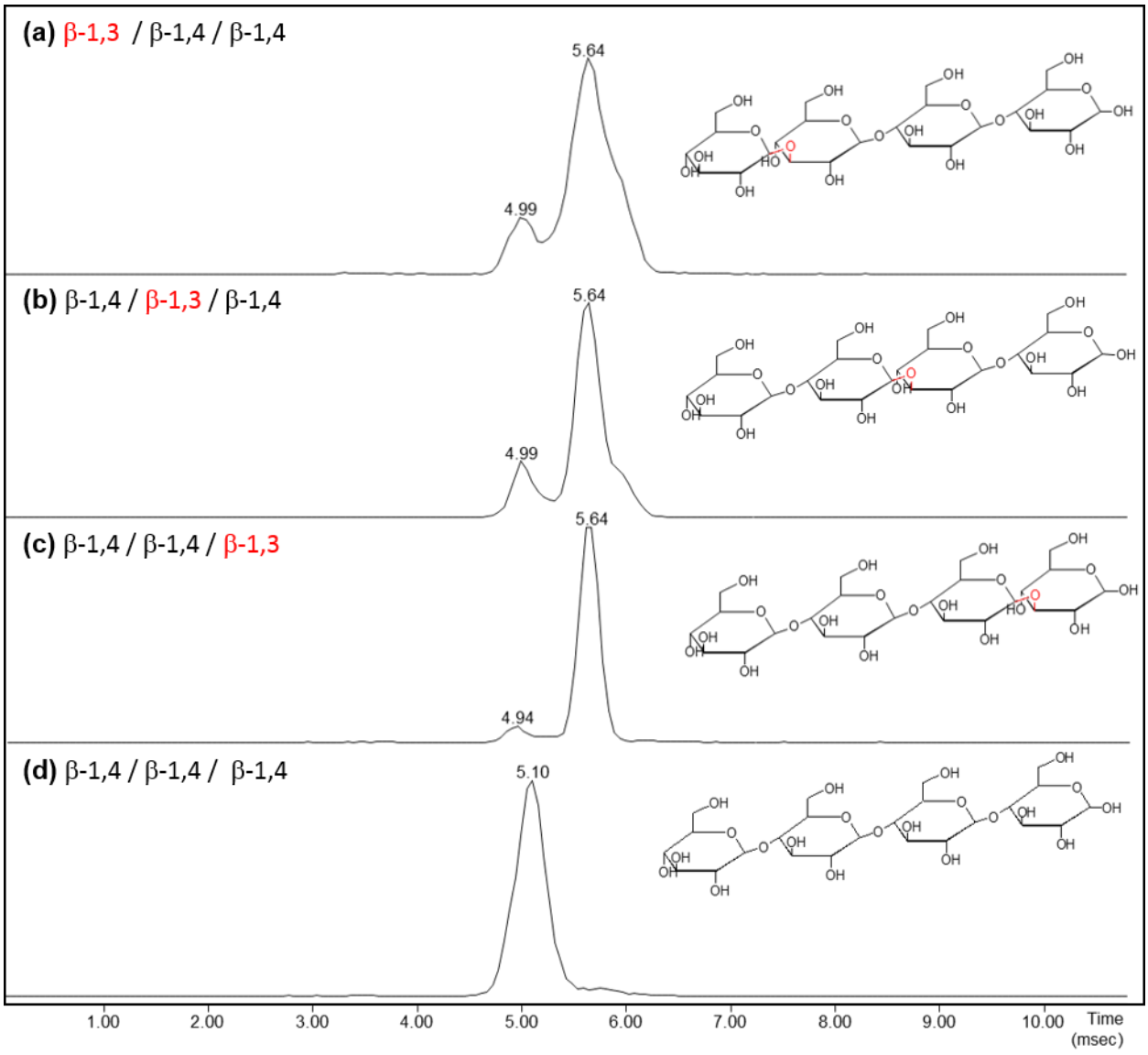

Figure 7: Ion mobility spectra on mixed-linked tetrasaccharide standards and cellulose DP4 (all ($[M+Na]^+$, $C_{24}H_{42}O_{21}Na$, *m/z* 689.21). Sequence order of glycosidic linkages is presented in the top left corner of each subplot.

Arrival time distributions (ATDs) from IM-MS recorded for the precursor at *m/z* 689.2 exhibited a single isoform for the pure β-1,4 cellulose DP4 with an arrival time of 5.1 msec (Figure 7d). In contrast, ATDs for the precursor at *m/z* 689.2 of the three mixed-linked tetrasaccharides indicated the presence of one or more impurities in all the tetrasaccharide standards (Figure 7a-c). The main isoform has an arrival time of 5.64 msec in all three samples. Based on the precursor mass and ion mobility measurement at this resolution, each mixed-link isomer is indistinguishable from the others. However, the ATDs in Figure 7a-c clearly show the presence of impurities that are isobaric with, but have measurably different ion mobilities

than, the mixed-linked tetrasaccharides at *m/z* 689.2. The impurities must therefore be branched impurities of have more than one β-1,3 linkage.

The ATDs serve as a measure of the degree of purity of the mixed-linked tetrasaccharides. A small-to-significant isoform at 5.0 msec in Figures 7a-c suggests a slight to significant contamination by a β-1,4 tetrasaccharide in each sample. In addition, the peak at 5.6 msec in Figure 7b contains a shoulder on the right-hand-side for the structure with the β-1,3 bond at position 2, and the same shoulder is even more apparent in Figure 7a with the β-1,3 bond at position 1. The shapes of the ATDs testify the occurrence of a greater diversity of conformers or linkages in these samples than initially expected. However, as described below, the correlation between the diversity of structures in the ATD and the unexpected abundance at the $^{3,5}A_n$ positions indicates that the diversity of structures in the ATD is more likely to be due to aberrant linkages rather than dispersity in gas phase conformations.

The proportion of contaminant isomers as revealed by ion mobility in each of the mixed-linked tetrasaccharides correlates with the intensity of fragment ions in He-CTD that did not match the expected linkage position (Figure 6). For example, for structure C, the ATD contains the purest isoform at 5.6 msec (Figure 7c). Accordingly, the He-CTD spectrum (Figure 6c) shows a pure structure with the β-1,3 glycosidic linkage in position 3 with a negligible peak at *m/z* 583 where the $^{3,5}A_4$ fragment would appear if a β-1,4 (or 1,6) linkage was present. The ratio of $^{3,5}A_3$ to $^{2,4}A_3$/ $^{0,2}X_2$ exceeds 1 for the other linkages, just like the cellulose standards (Figures 1 and 2). Concerning the structure B in Figure 7b, the contamination at 5.0 msec is more pronounced and the shoulder around 6.0 msec is also more pronounced. The corresponding He-CTD spectrum (Figure 6b) provides a ratio for the intensity of the $^{3,5}A_3$ and $^{1,3}A_3$ /$^{2,4}A_3$/ $^{0,2}X_2$ fragments of 0.3. The minor $^{3,5}A_3$ peak in this isomer indicates that the major structure has the expected β-1,3 glycosidic linkage at position 2 and that the contaminants present have either a 1,4 or 1,6 linkage at this position. The latter is supported by the presence of a $^{3,5}A_3$ fragment ion, which cannot arise from either 1,2- nor 1,3-linked carbohydrates. The peak at 5.0 msec and the shoulder of the dominant peak in the ATD of structure A in Figure 7a indicate that this isomer has the largest contribution of mixed-link impurities. This isomer yielded the most ambiguous ratio of $^{3,5}A_4$ to $^{2,4}A_4$/ $^{0,2}X_3$ of the three isomers (Figure 6a).

The evidence suggests that, in this case study, deviations from the expected ion ratios in the He-CTD spectra are caused by impurities of the mixed-linked isomers and not by inconsistencies in the performance of He-CTD itself. The quality of the structural information produced in He-CTD could be

334 further enhanced if He-CTD was coupled with liquid chromatography or ion mobility to address the issue
335 of heterogeneous mixtures of carbohydrates.

Conclusion

He-CTD can be used to determine the connectivity, i.e. the position of the glycosidic bond, of β-1,3- and β-1,4-linked native carbohydrates. The same He-CTD capabilities have not yet been tested in such detail for linkages with different anomericity (e.g. β-1,3 versus α-1,3) or different connectivity (e.g. β-1,3 versus β-1,6). One characteristic of He-CTD that enables such unambiguous structural characterization is the demonstration that consecutive fragmentations are not observed in the He-CTD product ion spectra. Although He-CTD creates high energy, radical, cross-ring cleavages, fragmentation does not continue past the primary fragments, and cleavages at multiple sites are not observed.

The abundance of specific cross-ring fragments from He-CTD depends on the position of the respective glycosidic bond. Although relatively low in intensity, the comparison of the abundance of cross-ring fragments to other cross-ring fragments provides a simple tool to assign connectivity. In the few examples that provided slightly ambiguous ratios for the expected β-1,3 linkages, ion mobility spectrometry confirmed that the ambiguity was proportional to the abundance of impurities in the mixed-linked standards. To be able to fully use the potential of He-CTD activation on complex mixtures, an efficient separation technique such as IMS would be required. Coupling He-CTD to IMS holds a number of advantages as IMS can distinguish compositional isomers, e.g. glucose from galactose [36] and multistage high-resolution ion mobility can discriminate anomers and distinguish isomeric fragment ions from both ends of the molecule.[37, 38] Although IMS-CTD would need to be demonstrated experimentally, an analytical instrument combining IMS prior to He-CTD fragmentation and permitting high-resolution ion mobility on precursor and fragment ions would enable unprecedented structural information on each peak/conformer in an arrival time distribution. In addition, the activation times in He-CTD are compatible with condensed-phase separation techniques such as hydrophilic interaction chromatography (HILIC), porous graphitic carbon (PGC) and electrophoretic separation methods, so any of these condensed-phase separation approaches could also be coupled to resolve the question about the identity of the isobaric impurities in a sample. On-line HPLC-CTD-MS or IMS-CTD-MS therefore has significant potential for the structural elucidation of unknown and complex oligosaccharides.

Author information

Corresponding authors

*Glen P. Jackson, Email: glen.jackson@mail.wvu.edu

*David Ropartz, Email: david.ropartz@inrae.fr

ORCID

Hagen Buck-Wiese: 0000-0002-4807-5795

Mathieu Fanuel: 0000-0001-8384-8266

Manuel Liebeke: 0000-0002-2339-1409

Peter H. Seeberger: 0000-0003-3394-8466

Jan-Hendrik Hehemann: 0000-0002-8700-2564

Helene Rogniaux: 0000-0001-6083-2034

Glen P. Jackson: 0000-0003-0803-6254

David Ropartz: 0000-0003-4767-6940

Author Contributions

JHH and ML initiated the project. HBW, MF, GPJ and DR performed MS experiments. KLMH, APV and PHS synthesized pure standards. HBW, HR, GPJ and DR wrote the manuscript. All authors contributed to the interpretation of the results, reviewed the manuscript and have given approval to the final version.

Notes

The authors declare no competing financial interest.

Acknowledgements

This material is based upon work supported by the National Science Foundation (NSF) under Grant No. CHE-1710376. Any opinions, findings, and conclusions or recommendations expressed in this material are those of the authors and do not necessarily reflect the views of the NSF. HBW acknowledges support from the Max-Planck-Society for doctoral studies and research travel opportunities. PHS thanks the Max-Planck-Society for generous financial support. The authors thank Guillermo Cayon for help with figure design.

References

1. Laine, R.A.: Invited Commentary: A calculation of all possible oligosaccharide isomers both branched and linear yields 1.05 × 1012 structures for a reducing hexasaccharide: the Isomer Barrier to development of single-method saccharide sequencing or synthesis systems. *Glycobiology*. **4**, 759-767 (1994).
2. Julius, M.L.: Carbohydrate Diversity in Microalgae. Microalgae in Health and Disease Prevention, p. 133-144. (2018).
3. Clausen, H. and S.-i. Hakomori: ABH and Related Histo-Blood Group Antigens; Immunochemical Differences in Carrier Isotypes and Their Distribution1. *Vox Sang*. **56**, 1-20 (1989).
4. Liu, Y.-H., N. Fujitani, Y. Koda, and H. Kimura: Distribution of H Type 1 and of H Type 2 Antigens of ABO Blood Group in Different Cells of Human Submandibular Gland. *J Histochem Cytochem*. **46**, 69-76 (1998).
5. Patnode, M.L., Z.W. Beller, N.D. Han, J. Cheng, S.L. Peters, N. Terrapon, B. Henrissat, S. Le Gall, L. Saulnier, D.K. Hayashi, A. Meynier, S. Vinoy, R.J. Giannone, R.L. Hettich, and J.I. Gordon: Interspecies Competition Impacts Targeted Manipulation of Human Gut Bacteria by Fiber-Derived Glycans. *Cell*. **179**, 59-73 e13 (2019).
6. Heiss, C., J. Stacey Klutts, Z. Wang, T.L. Doering, and P. Azadi: The structure of Cryptococcus neoformans galactoxylomannan contains β-d-glucuronic acid. *Carbohydr Res*. **344**, 915-920 (2009).
7. He, H., Y. Wen, Z. Guo, P. Li, and Z. Liu: Efficient Mass Spectrometric Dissection of Glycans via Gold Nanoparticle-Assisted in-Source Cation Adduction Dissociation. *Anal Chem*. **91**, 8390-8397 (2019).
8. Cody, R.B., R.C. Burnier, and B.S. Freiser: Collision-Induced Dissociation with Fourier Transform Spectrometry. *Anal Chem*. **54**, 96-101 (1982).
9. Zaia, J.: Mass Spectrometry and Glycomics. *OMICS A Journal of Integrative Biology*. **14** (2010).
10. Deguchi, K., H. Ito, Y. Takegawa, N. Shinji, H. Nakagawa, and S. Nishimura: Complementary structural information of positive- and negative-ion MSn spectra of glycopeptides with neutral and sialylated N-glycans. *Rapid Commun Mass Spectrom*. **20**, 741-6 (2006).
11. Chen, X., Z. Wang, Y.E. Wong, R. Wu, F. Zhang, and T.D. Chan: Electron-ion reaction-based dissociation: A powerful ion activation method for the elucidation of natural product structures. *Mass Spectrom Rev*. **37**, 793-810 (2018).
12. An, H.J. and C.B. Lebrilla: Structure elucidation of native N- and O-linked glycans by tandem mass spectrometry (tutorial). *Mass Spectrom Rev*. **30**, 560-78 (2011).
13. Hoffmann, W.D. and G.P. Jackson: Charge transfer dissociation (CTD) mass spectrometry of peptide cations using kiloelectronvolt helium cations. *J Am Soc Mass Spectrom*. **25**, 1939-43 (2014).
14. Tang, Y., Y. Pu, J. Gao, P. Hong, C.E. Costello, and C. Lin: De Novo Glycan Sequencing by Electronic Excitation Dissociation and Fixed-Charge Derivatization. *Anal Chem*. **90**, 3793-3801 (2018).
15. Tang, Y., J. Wei, C.E. Costello, and C. Lin: Characterization of Isomeric Glycans by Reversed Phase Liquid Chromatography-Electronic Excitation Dissociation Tandem Mass Spectrometry. *J Am Soc Mass Spectrom*. **29**, 1295-1307 (2018).
16. Wong, Y.L.E., X. Chen, R. Wu, Y.L.W. Hung, and T.D. Chan: Structural Characterization of Intact Glycoconjugates by Tandem Mass Spectrometry Using Electron-Induced Dissociation. *Anal Chem*. **89**, 10111-10117 (2017).
17. Pu, Y., M.E. Ridgeway, R.S. Glaskin, M.A. Park, C.E. Costello, and C. Lin: Separation and Identification of Isomeric Glycans by Selected Accumulation-Trapped Ion Mobility Spectrometry-Electron Activated Dissociation Tandem Mass Spectrometry. *Anal Chem*. **88**, 3440-3 (2016).

18. Yu, X., Y. Huang, C. Lin, and C.E. Costello: Energy-dependent electron activated dissociation of metal-adducted permethylated oligosaccharides. *Anal Chem*. **84**, 7487-94 (2012).
19. Kornacki, J.R., J.T. Adamson, and K. Hakansson: Electron detachment dissociation of underivatized chloride-adducted oligosaccharides. *J Am Soc Mass Spectrom*. **23**, 2031-42 (2012).
20. Schaller-Duke, R.M., M.R. Bogala, and C.J. Cassady: Electron Transfer Dissociation and Collision-Induced Dissociation of Underivatized Metallated Oligosaccharides. *J Am Soc Mass Spectrom*. **29**, 1021-1035 (2018).
21. Klein, D.R., F.E. Leach, 3rd, I.J. Amster, and J.S. Brodbelt: Structural Characterization of Glycosaminoglycan Carbohydrates Using Ultraviolet Photodissociation. *Anal Chem*. **91**, 6019-6026 (2019).
22. Crittenden, C.M., E.E. Escobar, P.E. Williams, J.D. Sanders, and J.S. Brodbelt: Characterization of Antigenic Oligosaccharides from Gram-Negative Bacteria via Activated Electron Photodetachment Mass Spectrometry. *Anal Chem*. **91**, 4672-4679 (2019).
23. Ropartz, D., P. Li, G.P. Jackson, and H. Rogniaux: Negative Polarity Helium Charge Transfer Dissociation Tandem Mass Spectrometry: Radical-Initiated Fragmentation of Complex Polysulfated Anions. *Anal Chem*. **89**, 3824-3828 (2017).
24. Ropartz, D., P. Li, M. Fanuel, A. Giuliani, H. Rogniaux, and G.P. Jackson: Charge Transfer Dissociation of Complex Oligosaccharides: Comparison with Collision-Induced Dissociation and Extreme Ultraviolet Dissociative Photoionization. *J Am Soc Mass Spectrom*. **27**, 1614-9 (2016).
25. Plante, O.J., E.R. Palmacci, and P.H. Seeberger: Automated solid-phase synthesis of oligosaccharides. *Science*. **291**, 1523-7 (2001).
26. Niedermeyer, T.H. and M. Strohalm: mMass as a software tool for the annotation of cyclic peptide tandem mass spectra. *PLoS One*. **7**, e44913 (2012).
27. Strohalm, M., D. Kavan, P. Novák, M. Volný, and V. Havlíček: mMass 3: A Cross-Platform Software Environment for Precise Analysis of Mass Spectrometric Data. *Anal Chem*. **82**, 4648-4651 (2010).
28. Strohalm, M., M. Hassman, B. Kosata, and M. Kodicek: mMass data miner: an open source alternative for mass spectrometric data analysis. *Rapid Commun Mass Spectrom*. **22**, 905-8 (2008).
29. Domon, B. and C.E. Costello: A systematic nomenclature for carbohydrate fragmentations in FAB-MS/MS spectra of glycoconjugates. *Glycoconj J*. **5**, 397-409 (1988).
30. R Core Team, *R: A language and environment for statistical computing.* R Foundation for Statistical Computing: Vienna, Austria (2019).
31. Vachet, R.W., K.L. Ray, and G.L. Glish: Origin of Product Ions in the MS/MS Spectra of Peptides in a Quadrupole Ion Trap. *J Am Soc Mass Spectrom*. **9**, 341-344 (1998).
32. Sleno, L. and D.A. Volmer: Ion activation methods for tandem mass spectrometry. *J Mass Spectrom*. **39**, 1091-1112 (2004).
33. Rosenstock, H.M., M.B. Wallenstein, A.L. Wahrhaftig, and H. Eyring: Absolute Rate Theory for Isolated Systems and the Mass Spectra of Polyatomic Molecules. *Proc Natl Acad Sci U S A*. **38**, 667-678 (1952).
34. Marcus, R.A.: Unimolecular Dissociations and Free Radical Recombination Reactions. *J Chem Phys*. **20**, 359-364 (1952).
35. Zubarev, R.A., N.L. Kelleher, and F.W. McLafferty: Electron Capture Dissociation of Multiply Charged Protein Cations. A Nonergodic Process. *J Am Chem Soc*. **120**, 3265-3266 (1998).
36. Hofmann, J., H.S. Hahm, P.H. Seeberger, and K. Pagel: Identification of carbohydrate anomers using ion mobility–mass spectrometry. *Nature*. **526**, 241-244 (2015).
37. Ujma, J., D. Ropartz, K. Giles, K. Richardson, D. Langridge, J. Wildgoose, M. Green, and S. Pringle: Cyclic Ion Mobility Mass Spectrometry Distinguishes Anomers and Open-Ring Forms of Pentasaccharides. *J Am Soc Mass Spectrom*. **30**, 1028-1037 (2019).

38. Ropartz, D., M. Fanuel, J. Ujma, M. Palmer, K. Giles, and H. Rogniaux: Structure Determination of Large Isomeric Oligosaccharides of Natural Origin through Multipass and Multistage Cyclic Traveling-Wave Ion Mobility Mass Spectrometry. *Anal Chem*. **91**, 12030-12037 (2019).